Journal of the European Ceramic Society **14** (1994) 91–96

Damage Investigations in Unidirectional SiC-MAS.L Composite Materials under Quasi-Static Tensile Loading

M. Drissi-Habti, T. Despierres, J. Foubert & M. Gomina

LERMAT, URA CNRS No. 1317, ISMRA, 6 Bd du Maréchal Juin, 14050 Caen Cedex, France

(Received 6 July 1993; revised version received 10 January 1994; accepted 20 January 1994)

Abstract

A simple approach to the analysis of damage in CMCs is proposed. The mechanical behavior of unidirectional SiC-MAS.L glass–ceramic composite materials is investigated using quasi-static uniaxial tensile loading. The extent of damage in specimens subject to different prestresses is characterized by the total number of transverse matrix cracks, N, and the reduction in the longitudinal Young's modulus, E. It is shown that the exponential functions may be used to describe the variation of N and E with applied strain.

Das mechanische Verhalten eines einachsigen SiC-MAS.L Glasskeramik Verbundwerkstoffs wird durch Aufbringen einer quasistatischen, einachsigen Belastung untersucht. Die steigende Schädigung in vorbelasteten Proben wird bewertet anhand der steigenden Anzahl N transversaler Risse und der Verringerung des Elastizittsmoduls E in Längs-richtung. Es wird gezeigt, daß die Variationen von N und E exponentielle Funktionen der Dehnung sind. Der Widerstand des Materials gegenüber steigender Schädigung wird durch ein R-Kurven vergleichbares Konzept abgeschätzt.

Cet article propose une première approche de l'analyse de l'endommagement dans les composites à matrices céramiques (CMC). L'étude du comportement mécanique de matériaux unidirectionnels SiC-MAS.L est conduite sous traction uniaxiale en chargement quasi-statique. Le développement et l'extension de l'endommagement sont analysés sur des éprouvettes précontraintes. Le niveau d'endommagement est caractérisé par le nombre de fissures matricielles transverses, N, et par la diminution du module d'élasticité longitudinal, E. Les variations de ces deux paramètres en fonction de la déformation appliquée sont décrites par des fonctions exponentielles.

1 Introduction

The utilization of fiber-reinforced ceramic matrix or glass–ceramic matrix composites in parts aimed at high-performance thermomechanical applications, (as in the aerospace industry to replace superalloys at temperatures higher than 1000°C), requires that their damage tolerance be demonstrated and evaluated. Hence, the different damage mechanisms in these materials must be determined as a function of the applied stress level, and the effects of damage on the variations of the mechanical properties must be evaluated.

It is the aim of this work to identify the different damage mechanisms and their onset in a uniaxial tensile loading test for unidirectional SiC-MAS.L composite material. The variations of mechanical parameters as a function of the preselected stress level are correlated with the increase in the total number of transverse matrix cracks.

2 Materials and Experimental Tests

2.1 Materials

The materials have been fabricated by Aérospatiale (établissement de Bordeaux), using a fabrication route similar to the one reported by Prewo *et al.*[1] They are made of continuous SiC fibers (NLM 202 Nicalon type) and a MAS.L glass–ceramic matrix. The unidirectional bundles of SiC fibers were infiltrated with a slurry of composition $0{\cdot}5MgO–0{\cdot}5Li_2O–1Al_2O_3–4SiO_2$ obtained using a sol–gel route. The preimpregnated unidirectional plies were then stacked and hot pressed at a temperature of about 1300°C under an inert atmosphere. The hot-pressing temperature could be modulated to control the crystalline structure of the matrix.[2] The physical characteristics of the

Journal of the European Ceramic Society 0955-2219/94/$7.00

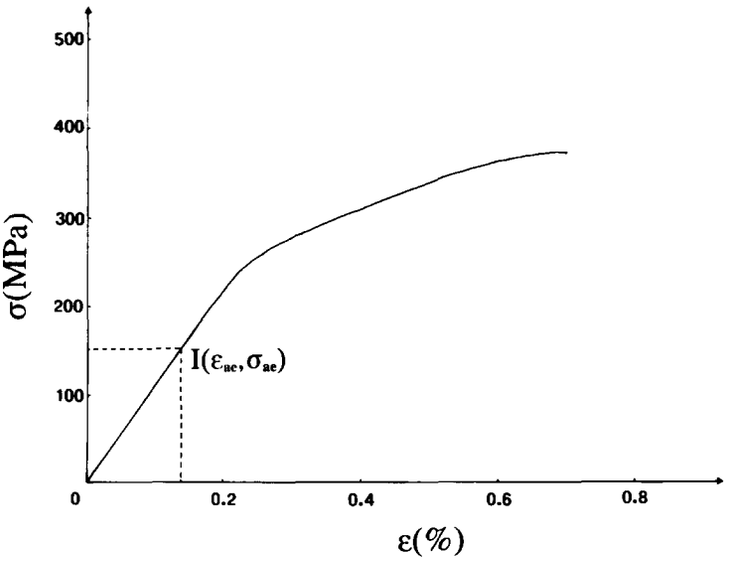

Fig. 1. Uniaxial tensile loading curve of a unidirectional SiC-MAS. L composite.

resulting composite materials are listed in Table 1 which include data from Ref. 2.

2.2 Experimental procedure

'Dog-bone' shaped specimens of total length l = 120 mm, with a gage length $L = 40$ mm and a cross-section S = 16 mm^2, were machined from as-processed plates. For each specimen one large face and a side face were finely polished using different grades of diamond paste (starting from grain size of 14 μm down to 1 μm). To prevent the slip of the specimens and an indentation of these soft-matrix materials, thin slices of a 2D SiC–SiC material were used to provide end tabs. The grips were specially designed for tensile tests on ceramic materials to minimize bending and shear moments using a triaxial rotation capability around the point of application of the load. Uniaxial tensile tests were conducted using a servo-hydraulic Schenck testing machine (Hydropuls PSB) with a 100 kN load cell. A strain gauge with a gauge length of 20 mm was clamped in the central zone of a large side of the specimens. A Dunegan 3000 acoustic emission detector equipped with a piezoelectric transducer of sensitivities of 30 to 50 dB between 25 kHz and 625 kHz was used to monitor the onset of damage and to record the cumulated number of acoustic emission signals during the test. A loading ramp rate of 400 N/min was used. Figure 1 shows a typical uniaxial loading curve for these materials. To investigate damage as a function of the applied stress, a set of specimens were loaded to different stress values σ_i. Once the predetermined stress value was reached, the specimen was unloaded (σ = 0) and then loaded again until the reloading loop meets the preceding unloading loop. This procedure is used to allow the measurement of the residual longitudinal Young's modulus on the reloading loop (E_r) or on the unloading loop (E_d). The specimen is then finally unloaded for microscopy observations. The damage introduced in the specimen is evaluated in terms of the total number of transverse microcracks N in the gauge length. The counting was performed inside a scanning electron microscope (Jeol T330). The

Table 1. Some physical characteristics of the unidirectional SiC-MAS.L composite materials

Composition of the matrix	$MgO–Li_2O–Al_2O_3–SiO_2$
Type of fiber	SiC, Nicalon NLM 202
Volume fraction of fibers	V_f = 0·33
Young's modulus of the fibers	E_f = 200 GPa
Young's modulus of the matrix	E_m = 70 GPa
Apparent density	ρ = 2500 kg/m^3
Number of plies	8
Longitudinal Young's modulus	123 GPa
Four-point bending strength	790 MPa
Tensile strength	400 MPa
Shear strength	16 MPa
Poisson's coefficient	0·23
Thermal expansion coefficient* (20 to 1000°C)	
Parallel to fibers	3·4 × 10^{-6}/°C
Perpendicular to fibers	1·7 × 10^{-6}/°C

* Data from Aérospatiale.

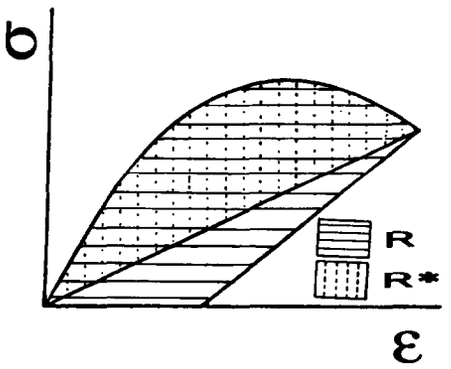

Fig. 2. Schematic of the method used to estimate the resistance of a composite to matrix multicracking.

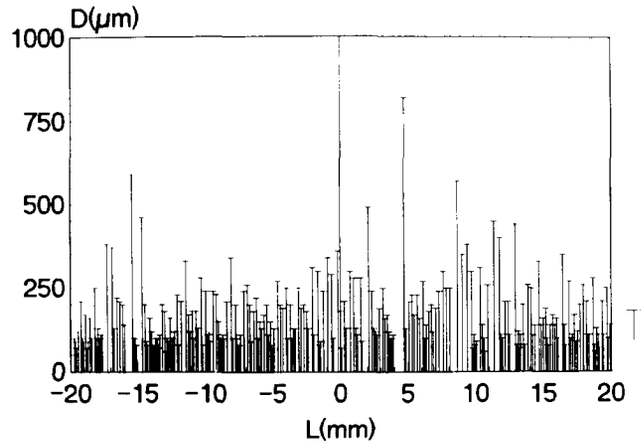

Fig. 3. Transverse cracks interspacing as a function of their position in the gage length for a strain value $\varepsilon = 0{\cdot}5\%$.

density of transverse microcracks $d = N/L$ was calculated and also the arithmetic mean crack spacing $\langle D \rangle$. The potential energy $R(\varepsilon_i)$ consumed for the creation of $N(\varepsilon_i)$ transverse microcracks is the area encompassed between the monotonic loading curve up to $\varepsilon = \varepsilon_i$ and the corresponding unloading loop (Fig. 2).

3 Results

3.1 Stress–strain curve

The correlation of the loading curve with the acoustic emission signals indicates that damage initiates at strain levels as low as $\varepsilon_{ae} = 0{\cdot}13\%$ (corresponding to $\sigma_{ae} \approx 154$ MPa). Meanwhile, the macroscopic behavior looks linear up to a strain of nearly 0·15% ($\sigma \approx 166$ MPa). Further, a domain of non-linear behavior extends from $\varepsilon = 0{\cdot}15$ to 0·30%. Beyond this domain, the linear behavior corresponds to a tangent modulus of 33 GPa. Because of the intensive multicracking in the plies, the stiffness of the matrix is considered to be negligible and hence, the application of the law of mixture leads to an effective volume fraction of intact fibers of 16·5% (half of the initial fibers

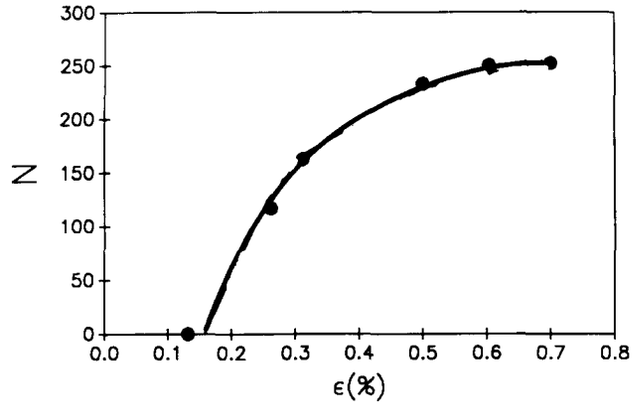

Fig. 4. Total number of transverse cracks in the gage length as a function of the strain.

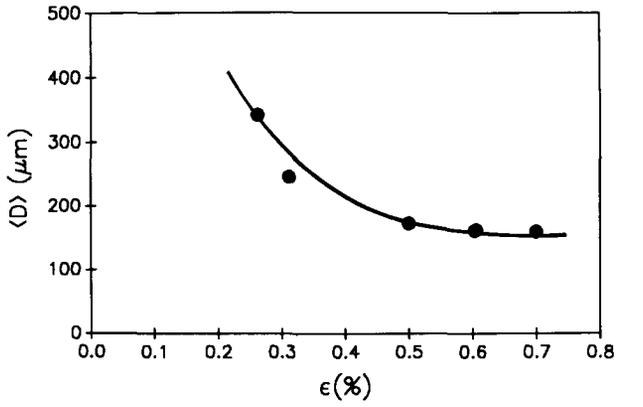

Fig. 5. Arithmetic mean crack interspacing as a function of the strain.

have failed). The remaining fibers progressively fail for strain values between 0·55 and 0·7%.

3.2 Characterization of damage

Figure 3 presents the crack interspacing D as a function of their position in the gage length, for a strain value $\varepsilon = 0{\cdot}5\%$. In Fig. 4 the number of transverse cracks N is shown to increase with the strain, up to $\varepsilon = 0{\cdot}5\%$. Beyond this strain value, this parameter reaches a saturation value $N_{sat} = 254$ and the crack density at saturation is $d_{sat} = 6{\cdot}3$ mm^{-1}; the mean crack interspacing $\langle D \rangle$ is then of 160 μm (Fig. 5). The intense microcracking in the plies is illustrated in Fig. 6 for a specimen loaded to rupture.

The variation of the number of transverse cracks as a function of the strain may be described by using expression (1) commonly employed for studying chemical kinetics:[3]

$$dN/d\varepsilon = (dN/dt)(dt/d\varepsilon) = k(N_{sat} - N) \quad (1)$$

the solution of which is:

$$N = N_{sat}\,(1 - \exp\,(\beta(\varepsilon - \varepsilon_0)) \quad (2)$$

where ε_0 the strain value corresponding to the

Fig. 6. SEM micrograph showing the intensive matrix microcracking in a specimen loaded to rupture.

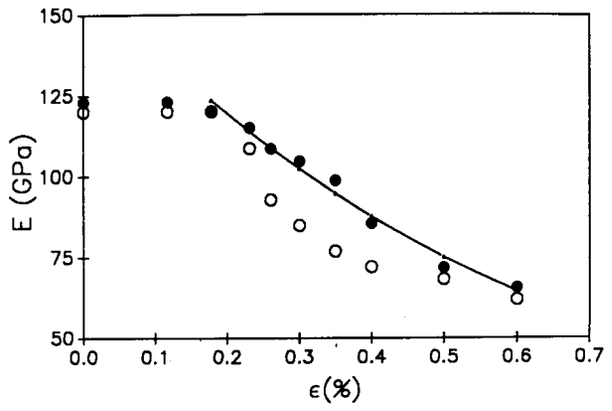

Fig. 7. Variation of the experimental Young's moduli as a function of the strain: (●) E_r measured on the reloading loop; (○) E_d measured on the final part of the unloading loop. The continuous curve is obtained from expression (3).

appearance of the first microcracks. The application of this expression to the experimental values of Fig. 4 gives $\beta = 6{\cdot}64$ and $\varepsilon_0 = 0{\cdot}15\%$. This latter value corresponds practically to the end of the linear elastic behavior.

Moreover, the decrease of the residual longitudinal Young's modulus measured on the linear part of the reloading loop (E_r) or on the unloading loop (E_d) is shown in Fig. 7. The accentuated decrease of E_d between $\varepsilon = 0{\cdot}25$ and $0{\cdot}5\%$ should be due to the presence of asperities at the surface of the fibers or to debris which impede fiber sliding.

The decrease of the residual modulus E_r assimilated into the longitudinal Young's modulus E, is apparent from a threshold value $\varepsilon'_0 = 0{\cdot}15\%$. It may be described by an exponential law:

$$E = E_0 \exp(-\alpha(\varepsilon - \varepsilon'_0)) \qquad (3)$$

where $\alpha = 1{\cdot}43$ and $\varepsilon'_0 = 0{\cdot}16\%$. The continuous decrease of the longitudinal Young's modulus as a function of the total number of transverse cracks N (Fig. 8) constitutes a relationship between a damaging parameter and a mechanical parameter easily usable for estimating the actual condition of a specimen.

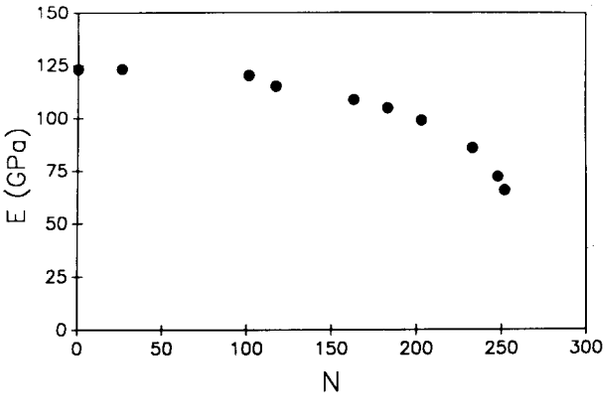

Fig. 8. Variation of the longitudinal Young's modulus as a function of the total number of transverse cracks.

4 Discussion

4.1 Damage evaluation

In this work the total number of transverse cracks have been chosen for the description of damage in these composite materials. The direct observation of the surface of the specimens during the test makes it possible to locate the sites of damage initiation and to follow its extent (growth of the microcracks, opening of the cracks). However, the detection of the cracks during the test is not reliable enough to account for the total number of transverse cracks because:

—The magnification of the optical microscope does not allow a fair identification of fine microcracks,
—any scratches remaining from polishing could be wrongly assimilated to cracks,
—it is absolutely necessary to follow the cracks all along the width of the specimen to avoid counting them more than once.

An alternative method which is widely used in the literature consists in making a replica of the surface while the specimen is still under load.[4] However, depending on the stress level adopted and the duration for the replica, new transverse matrix cracks (fatigue cracks) can be created and thus contribute to wrongly increase the number of cracks.

To prevent all these possible sources of experimental errors, a scanning electron microscope was used at a magnification $g > 750$ to document the development of matrix transverse cracks after the test.

Cracks running parallel to the fibers have not been included in the evaluation of damage although they may contribute somewhat to lower the longitudinal Young's modulus. These fine cracks are very difficult to document, because they are located at the fiber-matrix interface. It is supposed that they have no influence on the longitudinal strain, but they favor branching between the transverse cracks (Fig. 9).

4.2 Interfacial shear stress and surface energy of the matrix

Optical microscope and SEM observations indicate a rise in the number of transverse microcracks up to a strain value $\varepsilon \approx 0{\cdot}30\%$; a magnification of 1500 is sometimes necessary to show them. The kinetics of appearance of new transverse cracks decreases for $\varepsilon > 0{\cdot}40\%$ (Fig. 4). Beyond a strain value of $0{\cdot}50\%$, the creation of new cracks slows down strongly, the deformation of the specimen increases due to the opening of the microcracks already created, which attains 70 μm for speci-

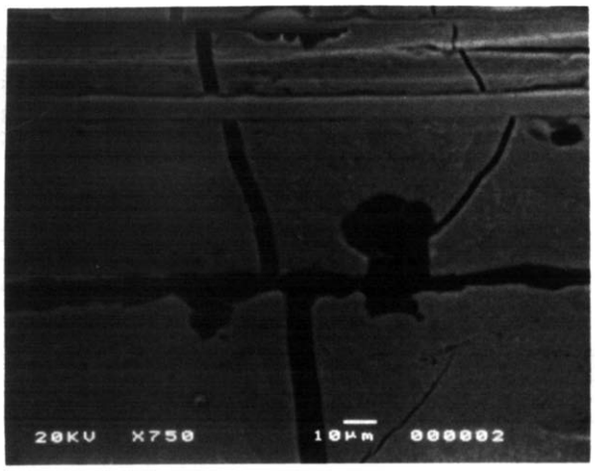

Fig. 9. SEM micrograph showing the branching of a crack running parallel to the fibers to transverse cracks.

mens stressed to rupture (Fig. 10). Pull-out lengths over 1 cm are frequently observed (Fig. 11). These observations support the hypothesis of the existence of a weak fiber–matrix interface. Thus, the interfacial shear stress has been evaluated using expression (4) derived by Aveston *et al.*:[4]

$$\tau = (V_m/V_f)(E_m/E_c)(r_f\sigma_a/2\langle D\rangle) \qquad (4)$$

where $V_f = 0{\cdot}33$ and $V_m = (1 - V_f)$ are the volume fraction of the fibers and the matrix respectively, σ_a = 154 MPa is the applied stress at the onset of first appearance of acoustic emission signals in the composite, r_f = 7·5 μm is the mean radius of the fibers and $\langle D\rangle_{sat}$ = 160 μm is the cracks interspacing at saturation. In this model it is assumed that the matrix undergoes microcracking at a constant applied stress level (while in the composite the matrix microcracking stress is distributed, due to the inherited flaws from elaboration). The calculated value of τ is 3·6 MPa. For the same composites, using an instrumented Vickers indenter, a value of 2 MPa have been obtained by Larnac *et al.*[2] By using an indentation method too but ana-

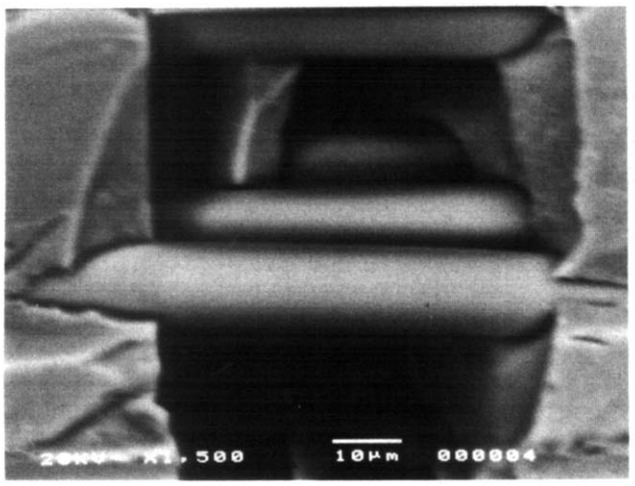

Fig. 10. SEM micrograph illustrating the drastic opening of transverse cracks in a specimen loaded to rupture.

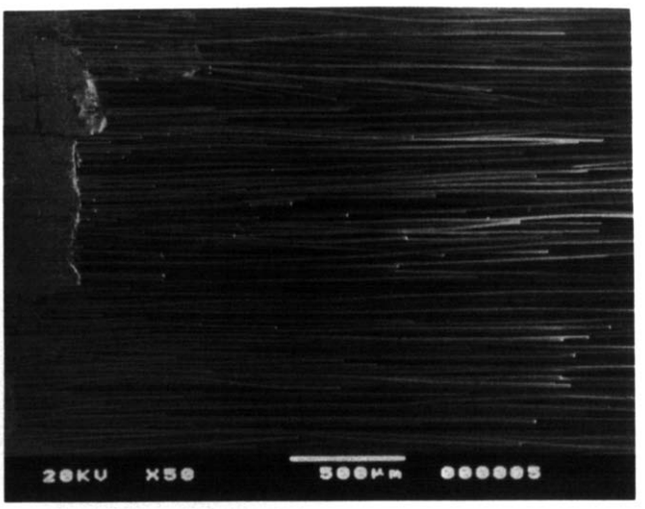

Fig. 11. SEM micrograph showing long pull-out lengths in these unidirectional SiC-MAS.L composites.

lyzing the results as a function of the fiber radius, Benoît *et al.*[6] have shown that for these materials the interfacial shear stress ranges between 0·5 and 8 MPa depending on the radius of the fibers. So, despite the fact that interface is induced differently in tensile tests and in indentation tests, the values obtained for τ using these two methods are compatible once the push-down tests are analyzed in terms of the size of the fibers. The relatively low value of τ is promoted by the presence of a thin layer of carbon (15 to 50 nm thick) which grows onto the fibers during the processing of the matrix,[2] and by a residual tensile stress due to the difference in the coefficients of thermal expansion of the constituants. The estimation of the elastic energy release rate Γ_m of the MAS-L matrix using expression (5):[5]

$$\varepsilon_m = (6\tau\Gamma_m E_f V_f^2/E_l\, E_m{}^2 r_f V_m)^{1/3} \qquad (5)$$

gives Γ_m = 9 J/m^2. This value is close to the one obtained by Pryce & Smith[7] from tensile tests for a SiC/CAS composite (Γ_m = 6 J/m^2) but is lower than those commonly reported for monolithic glass–ceramic matrices, which range between 15 and 30 J/m^2 by Beyerle *et al.*[9] This fracture energy of the glass–ceramic matrix leads to a toughness value $K_{Ic} \approx 1{\cdot}14$ MPa$\sqrt{\text{m}}$ which is reasonable for a glass–ceramic matrix.[9]

4.3 Resistance to multiple cracking

The total energy $R(\varepsilon_i)$ consumed to produce a strain ε_i is reported in Fig. 12 as a function of the strain ε. This energy includes the amount of energy necessary for (i) creating a number $N(\varepsilon_i)$ of transverse cracks corresponding to free surface energy of the matrix; (ii) friction of fibers; (iii) debonding at fiber–matrix interface; (iv) and rupture of fibers. It appears that the resistance to

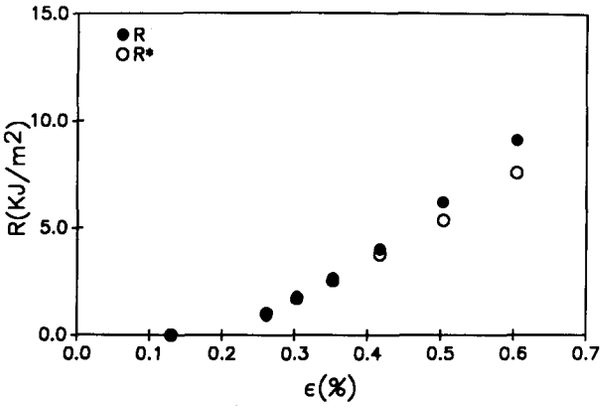

Fig. 12. Resistance to transverse matrix multicracking as a function of the strain.

the formation of transverse cracks is a continuously increasing function similar to the usual resistance curves encountered in fracture mechanics. This should be a practical way for making comparisons of different materials.

5 Concluding Remarks

In this paper, the accumulation of damage in a glass–ceramic matrix composite material is expressed in terms of the total number of transverse cracks, thus neglecting other sources of damage like some longitudinal cracks and the progressive failure of the weakest fibers. These precocious ruptures may influence both the orientation of the cracks and their interspacing.

The evolution of damage and the variation of the Young's modulus as a function of strain are dependent on two parameters β and α, investigations aimed to express β and α as function of the basic parameters of the materials (physical parameters of the constituents, geometric parameters linked to elaboration) are in progress.

In parallel to the concept of crack growth resistance curve widely used to describe the resistance of a material to crack propagation, a transverse microcracking resistance curve is defined for the comparison of different materials or the same materials obtained by different elaboration processes.

Acknowledgements

This work has been conducted within the joint research program GS4C of CNRS associating mainly Aérspatiale and the Société Européenne de Propulsion and a few French public laboratories. The authors thank Aérospatiale for machining and delivery of specimens.

References

1. Prewo, K. M., Brennan, J. J. & Layden, G. K., Fiber-reinforced glasses and glass-ceramics for high-performance applications. *Am. Ceram. Soc. Bull.*, **65**(2), 1986.
2. Larnac, G., Péres, P. & Donzac, J. M., Elaboration et caractérisation du composite à matrice vitro-céramique SiC/MAS-L. *Revue Hermés*, numéro spécial, Février 1993, pp. 27–41.
3. Despierres, T, Drissi-Habti, M. & Gomina, M., Damage characterization of 2D SiC–SiC composite material. *J. Eur. Ceram. Soc.*, in press.
4. Karandikar, P. G. & Chou, T. W., Damage development and moduli reductions in nicalon–calcium aluminosilicate composite under static fatigue and cyclic fatigue, *J. Am. Ceram. Soc.*, **76**(7) (1993) 1720–8.
5. Aveston, J., Cooper, G. A. & Kelly, A., Conference proceeding of the National Physical Laboratory, Teddington, UK. IPC Science and Technology Press Ltd, London, 1971, pp. 15–26.
6. Benoît, M., Brenet, P. & Rouby, D., Comportement des interfaces dans des composites céramique-céramique. *Composites et Matériaux Avancés*, numéro spéciale, Février 1993.
7. Pryce, A. & Smith, P., Behaviour of unidirectional and Crossply ceramic matrix composites under quasi-static tensile loading. *J. Mater. Sci.*, **27** (1992) 2695–704.
8. Beyerle, S. D., Spearing, S. M., Zok, F. & Evans, A., Damage and failure in unidirectional ceramic–matrix composites. *J. Am. Ceram. Soc.*, **75**(10) (1992) 2719–25.
9. Prewo, K. M., Fibre reinforced glasses and glass-ceramics. In *Glasses and Glass-Ceramics*, ed. M. H. Lewis, Chapman and Hall, 1989, pp. 336–68.